© 2019. Published by The Company of Biologists Ltd | Journal of Experimental Biology (2019) 222, jeb203091. doi:10.1242/jeb.203091

RESEARCH ARTICLE

Reorientation and propulsion in fast-starting zebrafish larvae: an inverse dynamics analysis

Cees J. Voesenek, Remco P. M. Pieters, Florian T. Muijres and Johan L. van Leeuwen*

ABSTRACT

Most fish species use fast starts to escape from predators. Zebrafish larvae perform effective fast starts immediately after hatching. They use a C-start, where the body curls into a C-shape, and then unfolds to accelerate. These escape responses need to fulfil a number of functional demands, under the constraints of the fluid environment and the larva's body shape. Primarily, the larvae need to generate sufficient escape speed in a wide range of possible directions, in a short-enough time. In this study, we examined how the larvae meet these demands. We filmed fast starts of zebrafish larvae with a unique five-camera setup with high spatiotemporal resolution. From these videos, we reconstructed the 3D swimming motion with an automated method and from these data calculated resultant hydrodynamic forces and, for the first time, 3D torques. We show that zebrafish larvae reorient mostly in the first stage of the start by producing a strong yaw torque, often without using the pectoral fins. This reorientation is expressed as the body angle, a measure that represents the rotation of the complete body, rather than the commonly used head angle. The fish accelerates its centre of mass mostly in stage 2 by generating a considerable force peak while the fish 'unfolds'. The escape direction of the fish correlates strongly with the amount of body curvature in stage 1, while the escape speed correlates strongly with the duration of the start. This may allow the fish to independently control the direction and speed of the escape.

KEY WORDS: 3D motion tracking, C-start, Escape response, Kinematics, Larval fish, Swimming performance

INTRODUCTION

The fast start is an important manoeuvre in the motion repertoire of many fish species across developmental stages (Domenici and Blake, 1997; Hale et al., 2002). Fast starts are commonly divided into two types by the shape changes of the fish during the motion: the S-start and the C-start. This article concerns the C-start, which is mainly used to escape from (potential) threats (Walker et al., 2005), and in some species for prey capture (Wöhl and Schuster, 2007). It involves the fish bending itself into a C-shape, and then unfolding to produce a strong acceleration and a change of direction (Hertel, 1966; Weihs, 1973). This motion is often considered to consist of three stages (Domenici and Blake, 1997; Hertel, 1966; Weihs, 1973): stage 1, where the fish bends into a C-shape; stage 2, where the fish unfolds; and stage 3, the remainder of the motion – continuous swimming or coasting. In this study, we looked at the first two stages of the C-start – we did not consider the highly variable third stage.

For the fast start to contribute to the survival of the larvae, the stages need to satisfy a number of functional demands (Voesenek et al., 2018). The primary demand on a start is to escape from a predator (Domenici and Blake, 1997). This requires strong accelerations to create sufficient distance in a short time between the predator and the larvae (Walker et al., 2005). In addition, it requires control over the escape angle, as the relative heading with respect to the predator often determines escape success (Domenici et al., 2011). As predators may approach from all sides, it is necessary that the larvae can produce a large range of possible escape directions, both horizontally and vertically. Finally, the threat should be detected early, and the response needs to be well timed for the escape to be effective (Stewart et al., 2013).

These functional demands should be fulfilled within physical constraints on the body of the larva and the hydrodynamics. To survive into adulthood, fish larvae need to be able to escape from predators immediately after hatching (Voesenek et al., 2018), while their muscles (Van Raamsdonk et al., 1978), sensory system and motor control (Fetcho and McLean, 2010) are not fully developed – even within these limits, the larvae need to respond appropriately and quickly, and produce effective motion. Furthermore, to perform effective propulsion as an undulatory swimmer, the larva needs to prepare its body for a propulsive tail-beat, in the case of a C-start by bending into a C-shape (Foreman and Eaton, 1993). To produce thrust, the fish also 'prepares' the surrounding water by generating (precursors to) vortices and jets that will contribute to the hydrodynamic forces in stage 2 (Ahlborn et al., 1991; Tytell and Lauder, 2008). In addition, stage 1 prepares the axial muscle for maximum power production by active lengthening of the contralateral side during bending (James and Johnston, 1998).

To meet the functional demands of the fast start, the fish larvae must generate hydrodynamic forces and torques, producing linear and angular accelerations. Different methods have been used to quantify hydrodynamic forces and torques during swimming. The motion of the fish and the flow can be quantified with high-speed video images and particle image velocimetry, allowing estimation of momentum changes of the fish and flow (Tytell and Lauder, 2008), or estimation of forces via a reconstructed pressure (Lucas et al., 2017). The reconstructed motion can also be used as input to a computational fluid dynamics method to estimate forces (Borazjani et al., 2012). Alternatively, the net forces and torques can be reconstructed from kinematics without requiring flow visualisation or fluid-dynamic models, based on inverse dynamics (Van Leeuwen et al., 2015; Voesenek et al., 2016). As the hydrodynamics are the only source of external forces and torques acting on the fish, we can use the net accelerations of the fish – both linear and angular – to calculate the hydrodynamic forces and torques directly from the kinematics.

Experimental Zoology Group, Wageningen University, PO Box 338, NL-6700 AH Wageningen, The Netherlands.

*Author for correspondence (johan.vanleeuwen@wur.nl)

C.J.V., 0000-0002-5467-8963; F.T.M., 0000-0002-5668-0653; J.L.v.L., 0000-0002-4433-880X

Received 7 March 2019; Accepted 23 June 2019

Journal of Experimental Biology (2019) 222, jeb203091. doi:10.1242/jeb.203091

The kinematics of the fast start have been characterised in many species (Domenici and Blake, 1993; Fleuren et al., 2018; Kasapi et al., 1993; Müller and Van Leeuwen, 2004). Fast starts have been stated to occur mostly in the horizontal plane (Domenici and Blake, 1997), and most studies investigate two-dimensional kinematics from single-camera high-speed video (e.g. Domenici and Blake, 1993; Harper and Blake, 1990; Hertel, 1966). However, three-dimensional kinematics studies show a vertical motion component in adults (Butail and Paley, 2012; Fleuren et al., 2018; Kasapi et al., 1993) and larval fish (Nair et al., 2015; Stewart et al., 2014). This vertical component is ecologically relevant, as it may influence the effectiveness of predator evasion with the escape response (Stewart et al., 2014).

In this study, we analysed fast starts of zebrafish larvae at 5 days after fertilisation. We filmed fast-start behaviour with a synchronised five-camera setup with high spatial and temporal resolution (Fig. 1A). From these videos, we reconstructed the kinematics in 3D (Fig. 1B,C) and used these data to calculate resultant hydrodynamic forces and torques. Based on the three-dimensional dynamics, we examined how zebrafish larvae meet the functional demands on the fast start. We show that zebrafish larvae produce torques in stage 1 that provide most of the reorientation of the body, while limited propulsion is produced. This is followed by a peak in propulsive force in stage 2, resulting in a strong acceleration of the centre of mass. The turn angle of a start is mostly determined by the amount of body curvature, while the speed at the end of stage 2 is mostly determined by the duration of the start. This allows early development larvae to perform appropriate escape responses for threats approaching from different directions and at different speeds.

MATERIALS AND METHODS

Animals

We used two batches (from different parents) of 50 wild-type zebrafish larvae, *Danio rerio* (Hamilton 1822), bred at the Carus animal facilities of Wageningen University. All fast-start sequences were filmed for fish at 5 days post-fertilisation, with a body length of 4.2±0.14 mm. We housed each batch in a separate tank, kept at a constant temperature of 27°C. The experimental aquarium was also maintained at 27°C by heating the experimental room. We placed 50 larvae at the same time in the aquarium. The fish were stimulated to perform fast-start manoeuvres by approaching them with a horse hair. Sequences where the hair touched the fish were eliminated from analysis, because the resultant forces would not only be from the hydrodynamics but also from the hair. However, the influence of the flow induced by the hair is limited: the centre of mass of the larvae

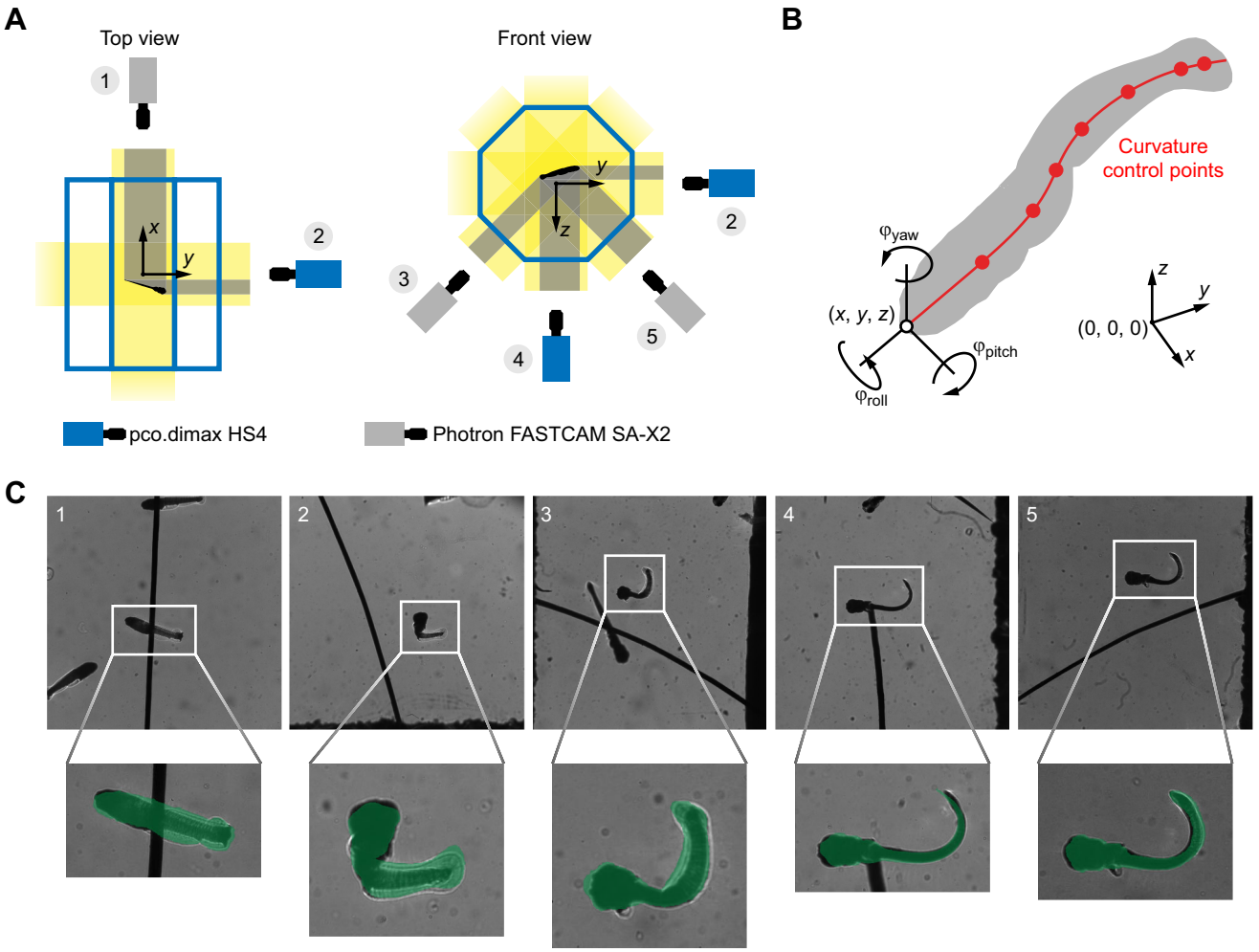

Fig. 1. Multi-camera setup and automated tracking method. (A) Sketch of the five-camera setup (top and front view). (B) Parameterised fish model used in the automated tracking method. The model parameters are the 3D position of the snout, the 3D orientation of the head as expressed by the Tait–Bryan angles (ϕ: roll, pitch and yaw), and a series of control points for the curvature along the body. Adapted from Voesenek et al. (2016). (C) Overlap between the high-speed video images (greyscale background) and projections of the body model (transparent green). The numbers in the top left corner correspond to the camera numbers in A.

hardly moves before the initiation of the start. All experiments were approved by the Wageningen University animal ethics committee.

Experimental setup

The swimming of larval zebrafish was recorded with a synchronised high-speed video setup with five cameras positioned at different orientations (Fig. 1A). Zebrafish larvae were placed in a glass aquarium in the shape of an octagonal prism (12 mm sides). To limit refraction effects, the cameras were placed perpendicular to the glass from five angles. From the bottom and the right side, we used pco.dimax HS4 cameras (PCO AG, Kelheim, Germany; 2000×2000 pixels). From the back, bottom left and bottom right side, we used Photron FASTCAM SA-X2 cameras (Photron, Tokyo, Japan; 1024×1024 pixels). All cameras were equipped with 105 mm f/2.8 macro lenses (105 mm f/2.8 FX AF MICRO-NIKKOR and AF-S 105 mm f/2.8G VR Micro, Nikon, Tokyo, Japan) with +5 dioptre close-up lenses [DHG Achromat Macro 200(+5), Marumi, Nagano, Japan], mounted on 27.5 mm extension tubes (PK-13, Nikon, Tokyo, Japan). All cameras were recording at 2200 frames s^{-1}, synchronised with a pulse generator (9618+, Quantum Composers, Bozeman, MT, USA). By using a collimated light setup, we created high-contrast shadow images with large depth of field. Collimated light was produced by shining an LED light source (MNWHL4/MWWHL4, Thorlabs Inc., Newton, NJ, USA) placed in the focus of a 250 mm lens (250D, Canon, Tokyo, Japan). The light setup was aligned such that the collimated light was parallel with the optical axis of the camera. As the fish larvae were in an aquarium between the light source and the camera, they projected deep shadows on a brightly lit background image at short shutter speeds (∼10 µs).

Camera calibration and modelling

We generated calibration points visible in all cameras by moving a sharp-tipped needle through the measurement volume with a computer-controlled micromanipulator (MCL-3, LANG GmbH & Co. KG, Hüttenberg, Germany). The needle was moved through a cuboid volume, at 5×5×5 uniformly spaced points along each dimension. This resulted in 125 images per camera with a known position of the needle tip. In each of these images, we indicated the needle tip manually with a custom-written Python 3 program (available on request from the corresponding author).

Camera projections were modelled by a simple affine transform, where we ignored perspective effects. For our camera setup, this is a valid assumption, as the shadows projected onto the sensor by the fish are (theoretically) independent of the distance from the sensor, owing to the collimated light. The affine transform for each camera was parameterised by a 3D translation and the orthonormal basis of the image plane coordinate system (i.e. one outward and two in-plane vectors). From an initial estimate of the camera parameters, we started a constrained optimisation procedure in MATLAB (interior-point algorithm as implemented in fmincon; R2016a, The Mathworks, Natick, MA, USA) (available on request from the corresponding author). Using this procedure, we minimised the sum of squared differences between the clicked image coordinates and the reprojected image coordinates, while maintaining orthonormality (i.e. all vectors perpendicular and of unit length) of the image plane basis vectors.

Motion reconstruction

The motion of the larvae was reconstructed from the synchronised high-speed video with the method described in Voesenek et al. (2016); it was originally developed in MATLAB, but converted to Python 3. We will briefly summarise the method here, but refer the reader to the original article for more details.

The method is based on a virtual representation of the camera setup and the fish larva. The virtual camera setup was created from the results of the calibration procedure described above. It transforms a point in world coordinates to image plane coordinates for each camera. The fish was represented by a 3D surface model. The shape, position and orientation of this model were determined by 14 parameters (3 for position, 3 for orientation, 8 for body curvature control points; Fig. 1B) – we ignored dorsoventral curvature, deformation of the median fin fold and motion of the pectoral fins. For every point in time, we applied the Nelder–Mead optimisation algorithm (Nelder and Mead, 1965) to these parameters to minimise the difference between virtual images, for which the 3D model was projected onto the virtual cameras, and the real high-speed video images, from which the fish was segmented. The result was a time series of body curvature along the body, position and orientation that described a 3D surface with optimal overlap (Fig. 1C). We smoothed each of these time series with regularised least squares (Eilers, 2003; Stickel, 2010), with derivatives of order 4 and a smoothing parameter of 100.

The reconstructed time series of parameters uniquely described the 3D shape of the fish. Under the assumption of a constant density across the fish, the mass distribution is known at every point in time. This allowed us to calculate its linear and angular momentum, and therefore the resultant fluid-dynamic forces and torques (Voesenek et al., 2016). In addition, for each frame in each tracked sequence, we determined visually from the bottom camera whether the pectoral fins were abducted or adducted.

Angle calculation

Similar to how the snout position does not correspond to the position of the centre of mass (Voesenek et al., 2018), the head angle is not representative of the overall orientation of the body. For this reason, we defined a body angle similar to Van Leeuwen et al. (2015) that is based on the angular momentum of the complete body, which we computed from the reconstructed motion of the fish (Voesenek et al., 2016). We calculated the body angle by integrating the angular velocity obtained from the angular momentum. We calculated the angular velocity as $\boldsymbol{\omega}=\mathbf{I}^{-1}\mathbf{L}$, where $\boldsymbol{\omega}$ is the angular velocity vector in rad s^{-1}, $\mathbf{I}$ is the moment of inertia tensor and $\mathbf{L}$ is the angular momentum vector. The moment of inertia tensor is obtained from the reconstructed 3D surface of the larvae (Dobrovolskis, 1996; Voesenek et al., 2016). We integrated the angular velocity vector with a custom-written MATLAB (R2018b) program (available on request from the corresponding author) implementing the midpoint rule (Simo and Wong, 1991; Zupan and Saje, 2011), a method for integrating 3D rotations that results in valid rotation matrices for each time step. For the first time step, we used the orientation of the head at the beginning of the start as the initial condition for the body angle. Finally, we reconstructed the body roll, pitch and yaw Tait–Bryan angles from these rotation matrices.

To summarise the curvature of the complete body in a single number, we used the head-to-tail angle. We define this as the angle between the first and last segment of the body (i.e. the head and the tail tip). As the body deformation angle is the integral of the curvature, the head-to-tail angle is equal to the mean curvature multiplied by the body length.

Statistics

For all statistical tests, we used a significance threshold of 0.05. We performed all statistics with MATLAB R2018b and the associated Statistics and Machine Learning Toolbox (R2018b, The Mathworks). We verified normality of the data with a Kolmogorov–Smirnov test (MATLAB's kstest). To calculate correlation coefficients, we fitted

Journal of Experimental Biology (2019) 222, jeb203091. doi:10.1242/jeb.203091

linear regression models (MATLAB's fitlm). We standardised all data before fitting the model by subtracting their mean and dividing by their standard deviation, which allowed us to use the fit coefficients as correlation coefficients (Schielzeth, 2010). To calculate confidence intervals of the correlation coefficients, we used bootstrapping with 10,000 repetitions, then calculated the 2.5th and 97.5th percentile. The correlation coefficients and their confidence intervals were converted into regression slopes by multiplying by σ_x/σ_y, the ratio of standard deviations.

For the models of the turn angle and speed as a function of the head-to-tail angle and duration, we initially fitted models with interaction terms between head-to-tail angle and duration. For both models, the correlation coefficients of the interaction terms were not significantly different from 0 (head-to-tail angle: P=0.069, N=33; speed: P=0.37, N=33), so we eliminated them from the model.

For selected pairs of variables, we performed total least-squares curve fits (Van Huffel and Vandewalle, 2006) with an optimisation method (MATLAB's fminsearch). To make these fits, we normalised both variables to a range of [0, 1]. We fitted functions of the form $y=c_1x^{c_2}$, as we expected a negative power law with an asymptote y=0 when $x\rightarrow\infty$. For each set of trial coefficients, we calculated the perpendicular distance to the curve for all data points. The squared sum of these distances was used as the objective function of the optimisation, resulting in a set of best-fitting coefficients c_1 and c_2. By bootstrapping with 10,000 repetitions and computing the 2.5th and 97.5th percentile, we calculated 95% confidence intervals of the coefficients.

RESULTS

Example of a fast start

We used an automated video-tracking method (Fig. 1) to reconstruct the fast-start motion of a zebrafish larva at 5 days after fertilisation, showing a change in direction of 83 deg and a maximum speed of 0.15 m s^{-1}. The larva curls into a C-shape in stage 1, then unfolds itself in stage 2 followed by a tail beat in the opposite direction (Fig. 2A). Over the course of the start, the larva reorients itself from being approximately aligned with the negative x-axis of the world reference frame, to swimming in the direction of the positive y-axis. In addition, it changes its pitch angle from a nose-down stance to an upward motion.

The reconstructed forces varied around 0 in stage 1 of the start, in the x-, y- and z-direction (Fig. 2B). Around the halfway point of stage 2, the force peaked, mainly in the 'forward' direction (i.e. the direction of the instantaneous velocity vector) – the larva pushes off and produces the largest acceleration, resulting in a velocity peak approximately 2 ms later (Fig. 2C). At the same time as the forward peak, an upward (i.e. positive z-direction) force peak also occurred, causing an upward velocity of the centre of mass (Fig. 2C). This was followed by a force peak in the opposite direction to the velocity, thus decelerating the larva.

The resultant torque in the z-direction in stage 1 is considerable (Fig. 2D) compared with the x- and y-torques. The z-torque can be interpreted as an approximate yaw torque as the deformation plane is approximately aligned with the x–y plane for the duration of the fast start (<10 deg deviation), while the smaller x- and y-torques together comprise the smaller out-of-plane (i.e. pitch and roll) torque. The first peak of the yaw torque in stage 1 reorients the fish, and is produced while the fish is bending into a C-shape. Later in stage 1, a counter-torque is produced that brakes the reorientation. In stage 2, a higher peak in the same direction as the counter-torque is produced to reorient the fish in the opposite direction during the push-off tail beat.

We determined body angles (Fig. 2E) by integrating the angular velocity that we calculated from the angular momentum and instantaneous moment of inertia. The head angles were defined with respect to the orientation of the stiff head region of the fish. The yaw angle was different as a result of the deformation of the larva – the head angle was not a good indicator of the orientation of the whole larva. The head angle showed large-amplitude variation across the start, while the body angle changed close to monotonically throughout the start, in the direction of reorientation. The pitch and roll angles also showed different dynamics between the head and body. Although the out-of-plane rotation caused by the pitch and roll angles was expected not to differ much between head and body coordinates, the values of the pitch and roll angles changed because they were coupled with the yaw angle, which did differ considerably.

Reorientation and speed

We determined the turn angle of the start by calculating the angle between the initial orientation of the larva and the heading at the end of stage 2. The initial orientation was defined as the unit vector pointing from tail tip to snout, while the heading was defined as the direction of the velocity vector of the centre of mass at the end of stage 2. The 'final speed' of the start was defined as the speed of the centre of mass at the end of stage 2. Fig. 3 shows the turn angle (Fig. 3A,B) and final speed (Fig. 3C,D) as a function of the head-to-tail angle and start duration. The head-to-tail angle was defined as the angle between the head and the tail at the transition point from stage 1 to stage 2, an indication of the whole-body curvature at the most-curved point. The start duration was computed as the time interval between start initiation and the end of stage 2.

More strongly curved starts showed a higher turn angle – the turn angle was strongly correlated to the head-to-tail angle, with a correlation coefficient of 0.83 [P<0.001, N=33; bootstrapped 95% confidence interval ($CI_{95\%}$): [0.71, 0.92]]. The slope of the regression was 0.59 deg ($CI_{95\%}$: [0.50, 0.65] deg) of turn angle per degree of head-to-tail angle. In contrast, the turn angle was weakly correlated with the start duration, with a correlation coefficient of 0.19 (P=0.032, N=33; $CI_{95\%}$: [0.028, 0.36]). A longer start duration tended to result in a slightly larger turn angle, at a rate of 0.84 deg ms^{-1} ($CI_{95\%}$: [0.125, 1.61] deg ms^{-1}).

Shorter starts had a higher final speed – the final speed was strongly negatively correlated with the duration of the start, with a correlation coefficient of −0.77 (P<0.001, N=33; $CI_{95\%}$: [−0.89, −0.63]). The slope of the regression was −0.0061 m s^{-1} per millisecond of the start – every millisecond shorter duration would result in a speed increase of 0.0061 m s^{-1}. We also fitted a power law to the final speed as a function of start duration, resulting in an exponent of −1.42 ($CI_{95\%}$: [−1.87, −1.05]). The final speed showed a weaker correlation with the head-to-tail angle, with a correlation coefficient of 0.38 (P=0.0033, N=33; $CI_{95\%}$: [0.11, 0.64]). The slope of the regression was 4.88×10^{-4} m s^{-1} ($CI_{95\%}$: [1.33×10^{-4}, 0.82×10^{-4}] m s^{-1}) per degree of head-to-tail angle; an increase in head-to-tail angle of 90 deg would result in an increase in final speed of 0.044 m s^{-1}.

The centrelines of the fish at the transition from stage 1 to stage 2 are shown in Fig. 3E, transformed to the coordinate system attached to the head of the fish in its initial orientation. The larvae curl up while the centre of mass remains in approximately the same position. The more strongly curved motions show a larger reorientation of the head, as well as a larger turn angle. In general, the head angle at the end of stage 2 was larger than the turn angle at the end of stage 2: the head turns further than the final heading at the end of stage 1, and then turns back over the course of stage 2.

Journal of Experimental Biology (2019) 222, jeb203091. doi:10.1242/jeb.203091

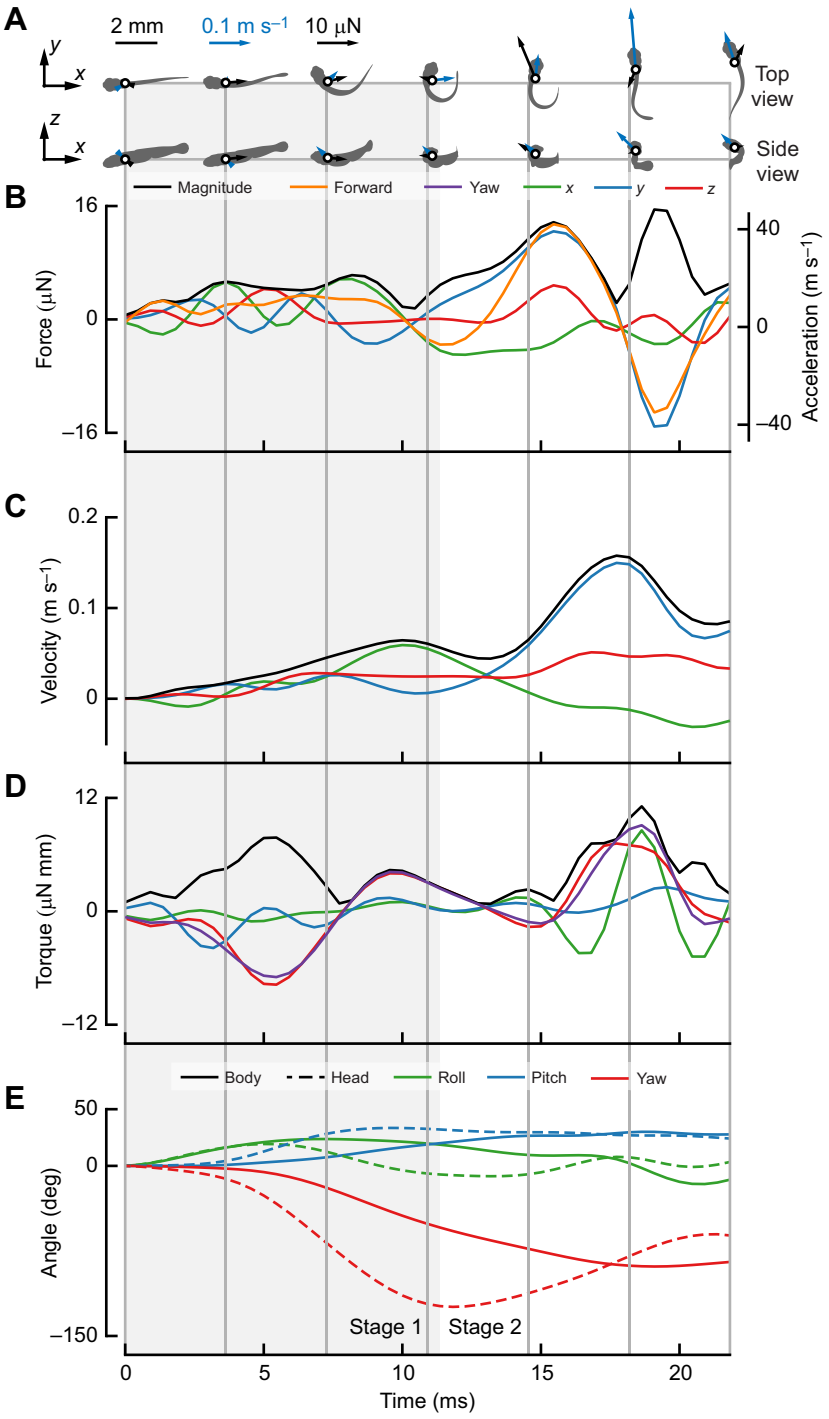

Fig. 2. Individual example of a fast-starting zebrafish larvae. Across all sub-panels, the light grey rectangle indicates stage 1, and the vertical dark grey lines connect the fish shapes in A to the time series in B–E. (A) Projections of the reconstructed fish model in the *x*–*y* (top) and *x*–*z* (bottom) plane. The white dot indicates the centre of mass, the blue arrow indicates the instantaneous velocity and the black arrow represents the instantaneous resultant force. (B) The instantaneous resultant force in the *x*, *y*, *z* and forward direction, and the force magnitude. The forward direction is defined as the vector pointing in the direction of the instantaneous velocity of the centre of mass. (C) The velocity of the centre of mass in the *x*, *y* and *z* direction, and the velocity magnitude. (D) The instantaneous resultant torque in the *x*, *y*, *z* and yaw direction, and the torque magnitude. The yaw torque is defined as perpendicular to the deformation plane of the centre line. (E) The body (solid) angle and head (dashed) Tait–Bryan angles: roll, pitch and yaw.

We can divide the total angle change of the body during the start into an elevation angle change (vertical reorientation) and an azimuth angle change (horizontal reorientation) (see Fig. 3F,G). The elevation change ranged from −35.0 to 34.2 deg (Fig. 3F); the azimuth change ranged from 3.9 to 102.7 deg (Fig. 3G). There was no significant correlation between the final speed and the azimuth change (P=0.77, N=33) or between final speed and the elevation change (P=0.13, N=33).

Stages of the fast start

We divided the fast start into stages following the same method as Fleuren et al. (2018), and analysed the first two stages. The durations of stage 1 and stage 2 were significantly correlated (P<0.001, N=33; correlation coefficient 0.79, $CI_{95\%}$: [0.70, 0.89]). Stage 1 took on average 52±4.6% of the start duration until the end of stage 2 (Fig. 4A) – slightly over half of the first two stages was spent bending into a C-shape. No starts were recorded where stage 1 took less than 42% or more than 64% of the start duration. The larvae showed a displacement between 3.3 and 21.1 times larger in stage 2 than in stage 1 (Fig. 4B). Also, the speed was greater (Fig. 4C), in terms of both total speed (1.5–5.6 times) and speed in the direction of the final heading (‘forward’, 1.7–23.6 times). The total speed in stage 1 was higher than the forward speed – the centre of mass moves slightly in stage 1, but not much in the forward direction (i.e. in the direction of the velocity at the end of stage 2).

Journal of Experimental Biology (2019) 222, jeb203091. doi:10.1242/jeb.203091

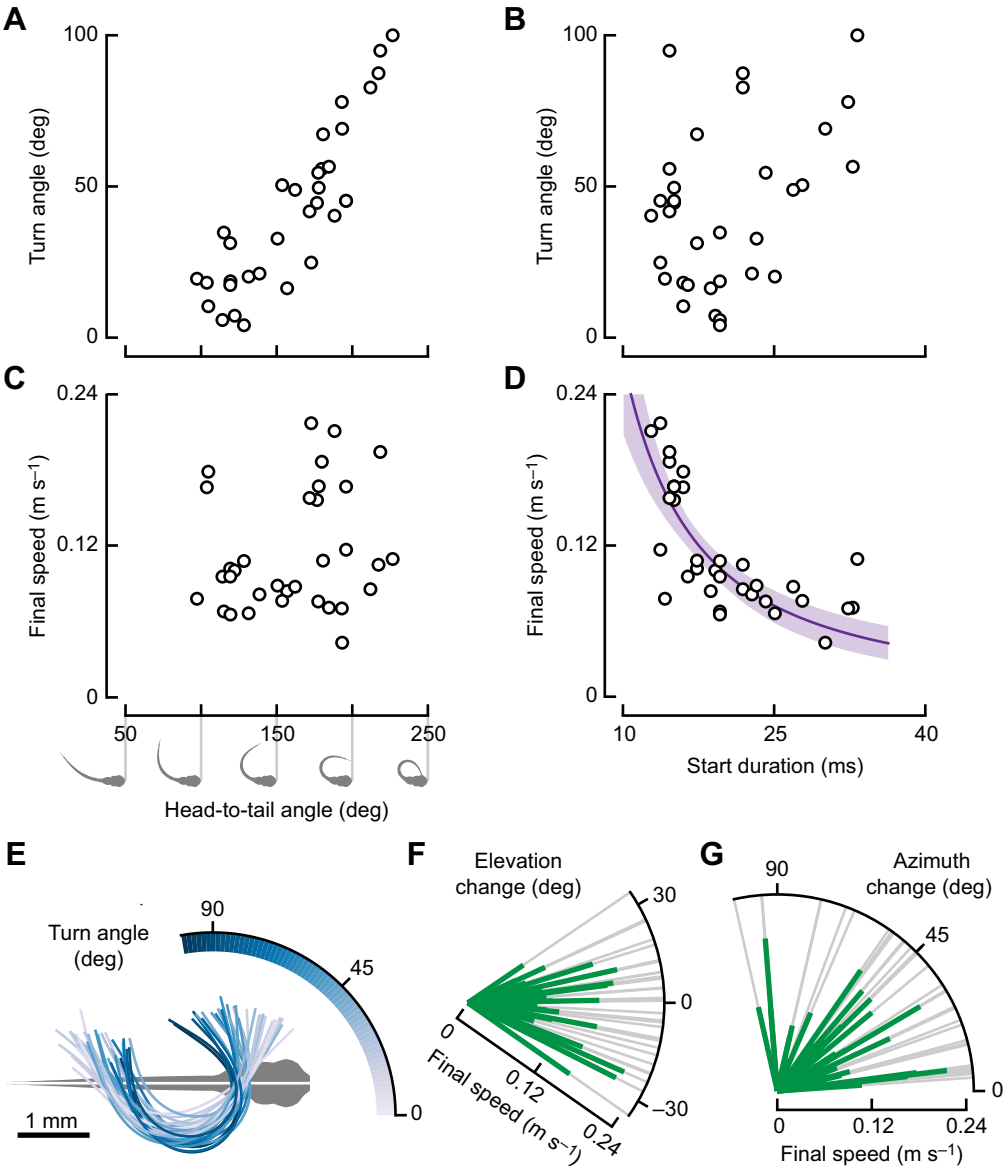

Fig. 3. Higher start curvatures increase turn angle, while shorter start durations increase final speed. (A,C) The turn angle (A) and the final speed at the end of stage 2 (C) as a function of the maximum head-to-tail angle, an indication of the total amount of curvature of the body, as illustrated below the horizontal axis of C. (B,D) The turn angle (B) and the final speed at the end of stage 2 (D) as a function of the start duration (computed as the time interval between start initiation and the end of stage 2). The purple line is a total least-squares curve fit of a power law with its 95% confidence interval (purple shaded area). (E) The shape of the centreline at the transition from stage 1 to stage 2, coloured by the turn angle of the start. (F) The elevation change (curved axis) and final speed at the end of stage 2 (green radial lines) for all analysed starts. (G) The azimuth change (curved axis) and final speed at the end of stage 2 (green radial lines) for all analysed starts. For all panels: *N*=33.

In all cases, the peak linear momentum was larger in stage 2 than in stage 1 (Fig. 4D; 1.5–5.6 times), while the peak angular momentum was often smaller in stage 2 than in stage 1 (Fig. 4E; 0.58–1.9 times). Stage 1 therefore often showed higher angular velocities than stage 2. In most cases, the peak force was higher in stage 2 than in stage 1 (Fig. 4F), for both the total force (0.80–4.6 times) and the 'forward' force (i.e. in the direction of the velocity at the end of stage 2; 0.82–10.3 times). Not much force was produced in stage 1, especially in the direction of the start – the acceleration was mostly visible as an undirected wiggling of the centre of mass. In most cases, the torque was also higher in stage 2 than in stage 1 (Fig. 4G; 0.78–3.9 times), but the ratio was smaller than that for speed and forces; some sequences even showed higher torques in stage 1 than in stage 2. The higher torques in stage 2 were presumably produced by the higher forces during the push-off.

Reorientation

Stage 1 had a significantly higher contribution to the yaw angle change than stage 2 (Fig. 5A; *t*-test, $P<0.001$, $N=33$); on average, the contribution of stage 1 was 28.7±13.7 deg higher than the contribution of stage 2. For smaller total yaw changes, stage 2 might have a negative contribution, undoing part of the reorientation of stage 1. Phase plots of the yaw angle (Fig. 5B) show that starts with relatively small turn angles generally have a negative contribution of stage 2 to the body yaw angle, while for large turn angles, the body yaw angle changes almost monotonically. In contrast, the head yaw angle showed considerably larger variation over the fast start than the body angle, reaching a maximum near the end of stage one, before rotating in the opposite direction in stage 2.

For all fast starts, we averaged the linear momentum, angular momentum and change in moment of inertia normalised by their maximum value (Fig. 5C–E). The linear momentum (Fig. 5C) reached a small peak in stage 1, followed by a much larger peak in stage 2, where peak speed was reached. In contrast, the angular momentum (Fig. 5D) showed its largest peak in stage 1, followed by a lower peak in stage 2. The large peak in angular momentum continued to the dip in moment of inertia (Fig. 5E). A combination of large angular momentum and low moment of inertia led to a high angular velocity, indicating a strong reorientation in stage 1. The subsequent reduction in angular momentum indicates that the yaw rotation is braked by a counter-torque; it then rose again as the fish beat its tail in the opposite direction.

Journal of Experimental Biology (2019) 222, jeb203091. doi:10.1242/jeb.203091

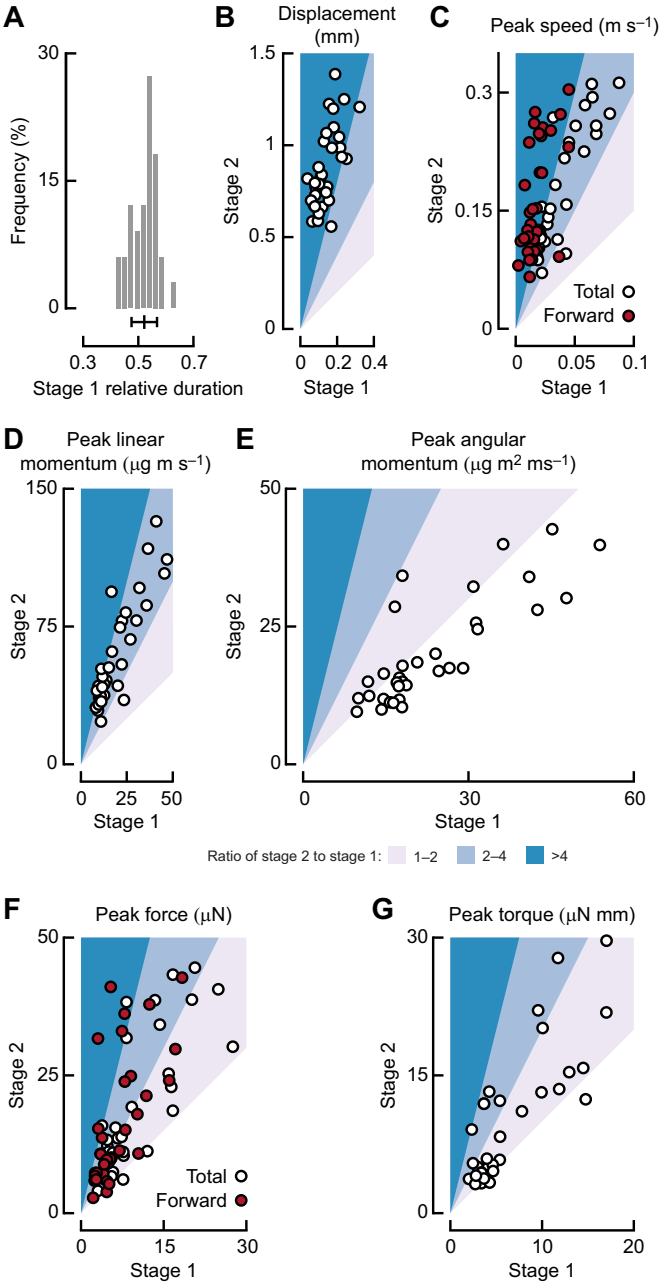

Fig. 4. Highest speeds, forces and torques occur in stage 2. (A) The duration of stage 1 with respect to the duration of the start (computed as the time interval between start initiation and the end of stage 2); the histogram indicates the frequency of each bin as a percentage of all starts. The bar below the histogram shows the mean±1 s.d. (B–G) The white region indicates where the values in stage 2 are lower than those in stage 1; the values for stage 2 are 1–2 times higher in the light blue region, 2–4 times higher in the medium blue region and >4 times higher in the dark blue region than those in stage 1. The *x*-axis shows the contribution of stage 1; the *y*-axis shows the contribution of stage 2. (B) Net displacement, i.e. the reduction in distance to the final position of the centre of mass at the end of stage 2. (C) Peak speed; white dots indicate the total speed, red dots indicate speed in the direction of the final heading. (D) Peak linear momentum. (E) Peak angular momentum. (F) Peak force; white dots indicate the total force, red dots indicate force in the direction of the final heading. (G) Peak torque. For all panels: N=33.

Propulsion in stage 2

We calculated the speed of the tail as the speed averaged over the posterior 10% of the body, relative to the speed of the centre of mass. The peak tail speed over the fast starts tended to increase with decreasing duration of the motion (Fig. 6A), with a correlation coefficient of −0.67 (P<0.001, N=33; $CI_{95\%}$: [−0.79, −0.54]). For every millisecond of decrease in duration, the peak tail speed increased by 20.3 m s^{-1} ($CI_{95\%}$: [16.3, 23.9] m s^{-1}). In addition, we fitted a power law to the tail speed as a function of start duration, resulting in an exponent of −1.27 ($CI_{95\%}$: [−1.68, −0.96]). As much of the propulsive force is produced at the tail, which moves in the opposite direction to the velocity of the centre of mass (Fig. 1A), the peak force tends to increase with increasing peak tail speed (Fig. 6B), with a correlation coefficient of 0.85 (P<0.001, N=33; $CI_{95\%}$: [0.70, 0.94]). The slope of the regression was 58.4 μN ($CI_{95\%}$: [48.3, 64.7] μN) per 1 m s^{-1} increase in tail speed. In this way, a decrease in duration leads to an increase in tail speed, and hence a corresponding increase in propulsive force, and therefore leads to an increase in escape acceleration.

Pectoral fin use during the fast start

For each time point in the fast start, we manually noted whether or not the pectoral fins were abducted. During high-speed starts, the pectoral fins remain adducted for the entire duration of the start, while during slower starts, they are abducted for part of the start (Fig. 7A). Whether the pectoral fins were abducted during a start did not depend on the turn angle (Fig. 7A). In starts where the fins were used, they were first abducted in stage 1 after 8.2±6.0% of the start duration (Fig. 7B). They were then adducted in stage two, after 75±8.3% of the start duration, resulting in an average duration of pectoral fin abduction of 67±8.6% of the start duration.

In starts where the fins were used, the fraction of the start during which they were abducted correlated significantly with the change in elevation (P=0.0252, N=17), with a correlation coefficient of 0.54 ($CI_{95\%}$: [0.15, 0.83]). In starts where the fins were not used, large elevation changes could also be produced – the mean elevation change between starts with and without fins was not significantly different (two-sample t-test, P=0.82, N_1=17, N_2=16).

DISCUSSION

We reconstructed the 3D motion of zebrafish larvae at 5 days after fertilisation during C-start escape responses and reconstructed linear and angular momentum, forces and torques. We consider the results of the analysis in the context of the functional demands of the start, as outlined in the Introduction.

Producing acceleration

The primary demand of a fast start is to accelerate the body, both linearly and rotationally. This acceleration is produced by a large force peak in stage 2 (Figs 2B and 4F), causing an increase in linear momentum, and hence speed (Figs 2C, 4D and 5C). Although the body is prepared for the propulsive stroke by curling up in stage 1, the body curvature (as expressed by the head-to-tail angle) correlates with the speed relatively weakly (Fig. 3C). In contrast, the speed shows a strong inverse correlation with the duration of the start, with a power law exponent of −1.42: shorter starts lead to higher speeds (Fig. 3D). The durations of stage 1 and stage 2 do not vary independently (Fig. 4A), similar to what was found by Nair et al. (2015). Hence, shorter start durations lead to shorter durations of stage 2, resulting in an increase in tail speed (Fig. 6A) with a power law exponent of −1.27, and a resulting increase in force (Fig. 6B).

To generate these forces, fish produce fluid-dynamic jets. During stage 1, fish larvae produce a jet flow into the C-shape (Li et al., 2014; Müller et al., 2008). A computational fluid dynamics simulation of a single zebrafish larva swimming sequence

Journal of Experimental Biology (2019) 222, jeb203091. doi:10.1242/jeb.203091

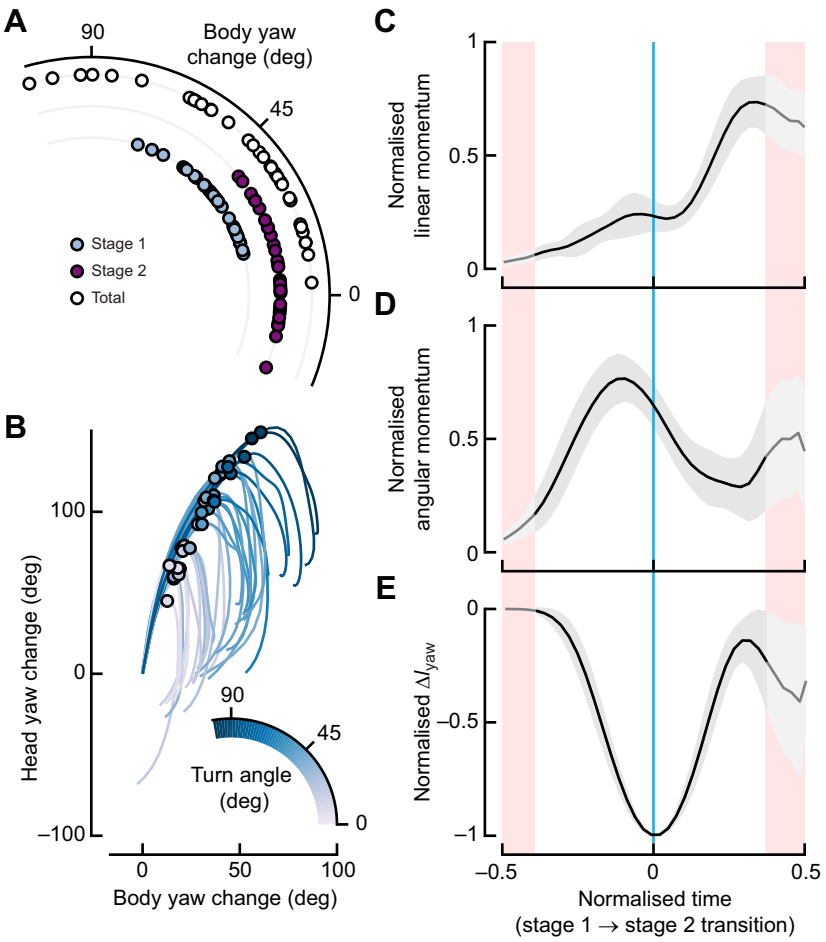

Fig. 5. Reorientation during the fast start. (A) Change in yaw angle in stage 1 (blue), stage 2 (purple) and the complete start (white). (B) Phase plots of the change in head yaw angle to the change in body yaw angle, coloured by the turn angle of the start (the angle between the initial orientation of the fish and the direction of the velocity vector at the end of stage 2). The dots indicate the transition point from stage 1 to stage 2. Each line traces the head yaw angle and body yaw angle through an individual fast start, starting at (0, 0). (C–E) The black line indicates the mean, with ±1 s.d. shown by the grey area. The translucent red bands on the left and right indicate time points for which not all data are present because of differences in the relative length of stage 1 and 2. The blue line indicates the transition point from stage 1 to stage 2. C–E show the linear (C) and the angular (D) momentum profile over the start, and changes in moment of inertia in the deformation plane (ΔI_{yaw}; E), normalised by the maximum absolute value and aligned to the transition from stage 1 to stage 2 before averaging over all starts. For all panels: *N*=33.

(Li et al., 2012) showed that initially this mainly produces a torque that reorients the fish. The jet is then reoriented along the body in stage 2, where it produces propulsive force, in agreement with our reconstructed resultant forces (Fig. 2B). Adult bluegill sunfish show a similar flow pattern in velocity field measurements (Tytell and Lauder, 2008).

Based on numerical simulations, it has been found that the motion of the larval C-start was near-optimal for maximising escape distance in a given time (Gazzola et al., 2012) – a measure that corresponds to maximising the mean acceleration during a start from a standstill. These authors also found that a greater curvature could result in a higher escape distance, for a given start duration; this corresponds to the weak correlation that we found for speed with head-to-tail angle. For (near-) cyclic swimming of larval fish, the swimming speed was found to increase with increasing tail-beat frequency and to a lesser extent amplitude (Van Leeuwen et al., 2015). The fast start duration is the equivalent of the frequency, while the head-to-tail angle is connected to the tail-beat amplitude. Hence, we saw similar effects on speed in fast starts as in cyclic swimming.

Reorienting the body

The larvae produce a wide range of escape directions (Fig. 3F,G), both in azimuth and, to a lesser extent, in elevation. The turn angle of a start correlates strongly with the head-to-tail angle: more strongly curved starts tend to show a larger turn angle (Fig. 3A,E).

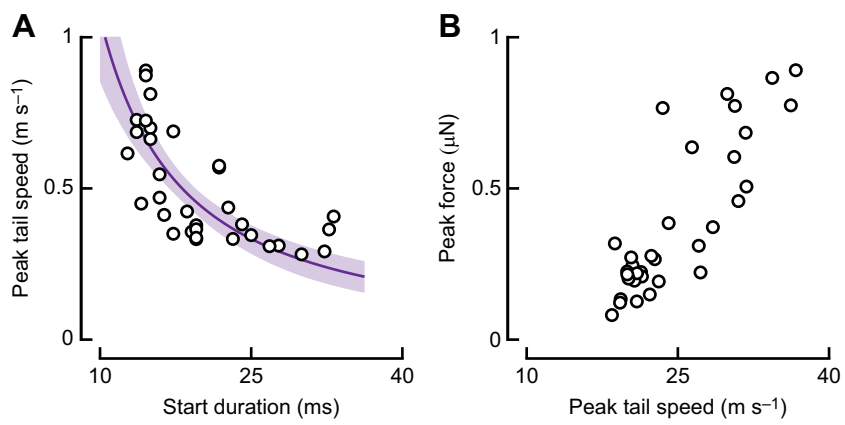

Fig. 6. Higher tail speeds with shorter durations lead to higher forces. (A) The peak tail speed in stage 2 as a function of the start duration. The purple line is a total least-squares curve fit of a power law with its 95% confidence interval (purple shaded area). (B) The peak force in stage 2 as a function of the peak tail speed in stage 2. For A and B: *N*=33.

Journal of Experimental Biology (2019) 222, jeb203091. doi:10.1242/jeb.203091

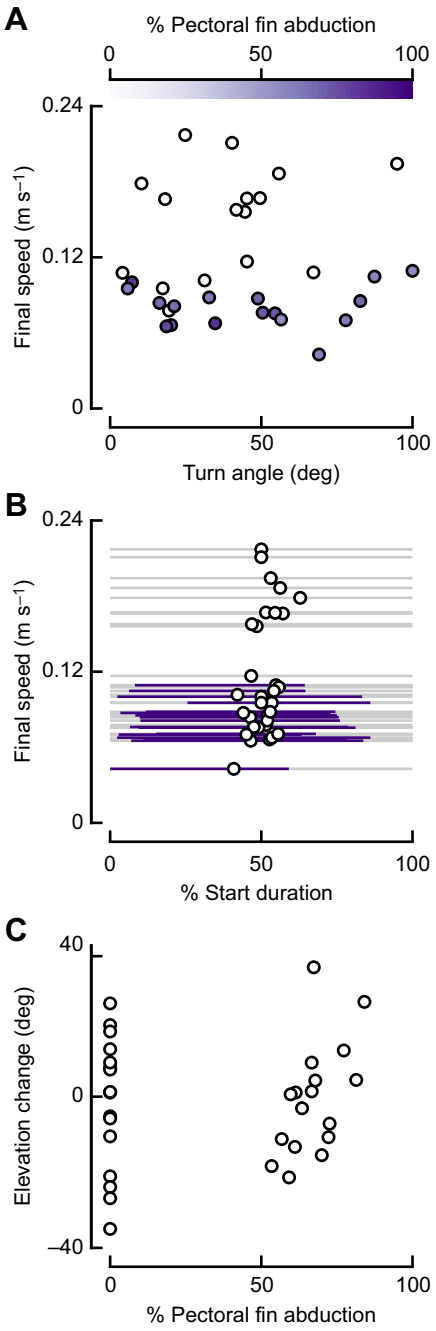

Fig. 7. Pectoral fins are only abducted during low-speed starts and help produce elevation change. (A) The percentage of the start duration (computed as the time interval between start initiation and the end of stage 2) that the pectoral fins are abducted (colours) in the turn angle–final speed parameter space. (B) The relative time (as a fraction of the start duration) that the pectoral fins are abducted (purple lines) as a function of speed. Each grey line indicates a start, with the transition point between stage 1 and 2 indicated by the dot. (C) The elevation change as a function of the percentage of the start that the pectoral fins are abducted. For all panels: *N*=33.

The turn angle correlates weakly with the duration of the start (Fig. 3B), where longer starts show a slightly larger turn angle. Hence, large turn angles do not take much more time to produce than small turn angles. In adult fish, the start duration correlates more strongly with the escape angle (angelfish: Domenici and Blake, 1991; goldfish: Eaton et al., 1988). This suggests a difference in reorientation between adults and zebrafish larvae: adults seem to use an approximately fixed turn rate, while larval zebrafish increase turn rate with increasing turn angle.

The changes in escape angle are mostly produced in stage 1 (Fig. 5A), despite lower peak torques (Fig. 4G). The yaw torque is consistently in the direction of turning during the first part of stage 1 (Fig. 2D), causing the angular momentum to show its largest peak in stage 1 (Fig. 5D), while the moment of inertia is close to its minimum (Fig. 5E). The high angular momentum combined with a low moment of inertia lead to a high angular speed, allowing large turn angles. At the end of stage 1, the torque reverses sign (Fig. 2D), thus reducing the angular momentum. Together with the increase in moment of inertia (Fig. 5E), this decreases the angular speed. The torque then decreases until the end of stage 2, where the torque increases again, rotating the fish in the opposite direction (Fig. 2D). This reorienting torque and the following counter-torque were shown to be caused mainly by pressure forces, while the largest shear forces were found at the head, and counteracted the initial reorienting torque (Li et al., 2012).

Previous studies of adult fish have shown that the turn angle of the head in stage 1 correlates with the turn angle during the complete fast start (Domenici and Blake, 1993; Eaton et al., 1988; Fleuren et al., 2018). This has also been found for fast starts of zebrafish larvae (Nair et al., 2015); in addition, the tail angle and the azimuth change during fast starts were found to be correlated. Large head and tail angles are caused by strong body curvature. Body curvature is summarised by the head-to-tail angle, which is proportional to the mean curvature along the body.

Danos and Lauder (2007) analysed routine turns of zebrafish larvae, for which they created a model where only bending of the body caused a change in head angle, resulting in a large underprediction of the escape angle. They suggested that the additional effect is caused by fins. In fast starts, however, the pectoral fins cannot explain the reorientation torque as they are adducted at high speeds, even for large turn angles (Fig. 7A). Without fins, fish have been shown to produce a yaw torque in the first stage of the start (Li et al., 2012; Song et al., 2018). This torque is mainly produced by pressure forces at the tail, which has a much larger lever arm with respect to the centre of mass than the pectoral fins.

Alternatives to the head angle

The head angle change after stage 1 is connected to the head-to-tail angle of the fish as a result of the stereotypical nature of the C-bend (Fig. 3E). The tail excursion of zebrafish larvae was found to correlate with the head yaw angle (Nair et al., 2015), so the head-to-tail angle correlates with the head yaw angle. Rather than use the head angle to indirectly indicate the curvature of the start, we use the head-to-tail angle as a more direct indicator of the whole-body curvature. As the posterior part of the fish produces much of the reorienting torque (Li et al., 2012; Song et al., 2018), it is useful to consider the complete body when analysing the escape direction.

Furthermore, rather than using the head angle as an indicator of orientation (Domenici and Blake, 1993; Eaton and Emberly, 1991; Nair et al., 2015), we used the ‘body angle’ that we calculated from the mass distribution. The head angle is not representative of the heading of the fish: they differ considerably across most of the fast start (Figs 2E and 5B). The body angle is more difficult to quantify than the head angle, as it requires a 3D mass distribution model of the fish, and reconstructed kinematics of high accuracy (Van Leeuwen et al., 2015). Nonetheless, it is worth calculating when analysing reorientations, as it gives a much more accurate representation of the reorientation of the fish mass. In the absence of body angles, the head angle cannot be used to replace it, as it shows completely different dynamics.

Control of the fast start

The turn angle and final speed seem to be adjusted mostly independently for C-starts of zebrafish larvae. The turn angle can be adjusted with the head-to-tail angle (i.e. body curvature), having relatively limited effect on the escape speed (Fig. 3A,C). The escape speed can be adjusted with the start duration, having a limited effect on the escape angle (Fig. 3B,D). In adult goldfish, the escape trajectory was found to be controlled by the relative size of the initial and second contractions and the timing between them, with minimal feedback from sensors (Foreman and Eaton, 1993). Assuming that starts are controlled similarly in larval zebrafish, the head-to-tail angle and start duration are presumably a direct result of these parameters, and might be used as proxies for them.

The duration of stage 1 and stage 2 varies concomitantly (Fig. 4A), as previously found for two species of adult fish (Webb, 1975) and zebrafish larvae (Nair et al., 2015). The larvae do not individually tune the duration of stage 1 and stage 2 to adjust the angle and speed of their escape. At a given escape speed, smaller head-to-tail angles are produced by turning more slowly, rather than turning at the same rate but over a shorter time. Furthermore, the duration of stage 2 is not shortened independently of stage 1 to increase the tail speed, and hence propulsive force. This might suggest a limitation on how quickly the tail-beat duration can be changed from one tail-beat to the next.

The elevation of the start has been found to be controlled by dorsoventral excursions of the midline (Nair et al., 2015). In the slow starts where the pectoral fins were used, the amount of time that the pectoral fins were abducted correlates with the elevation change (Fig. 7C). Larvae of 5 days post-fertilisation naturally show a nose-down pitch moment (Ehrlich and Schoppik, 2017), so a hydrodynamic torque must be produced to counteract this for positive, or perhaps even less-negative elevation changes. The action of the pectoral fins is an additional effect to the dorsoventral tail excursion, as starts without pectoral fin abduction do not produce significantly different elevation changes. The pectoral fins are only used during relatively slow C-starts (Fig. 7A). At lower speeds, perhaps the required pitch torques cannot be produced by the body alone, requiring the help of the pectoral fins. In contrast, at high speeds, the body is able to produce sufficient pitch torque, and can adduct the fins to reduce drag to achieve a higher escape speed.

Timing the start

The importance of fine-tuning the speed and direction of the escape depends on the speed of the predator relative to the prey. In adult guppies, it was shown that when the speed of the predator is close to the speed of the prey, faster starts will result in greater survival probability (Walker et al., 2005). In larval zebrafish, however, the speed and direction of the escape are less important for much higher or much lower predator speeds relative to the prey than for intermediate predator speeds (Soto et al., 2015). Zebrafish larvae have been classed as being in the 'slow-predator' regime, where escape timing, rather than escape speed, is the dominant parameter (Nair et al., 2017) influencing escape performance, although below a certain escape speed (>50% reduction), the probability of escape from the predator's suction flow drops rapidly (Nair et al., 2017).

Zebrafish larvae show a relatively long stage 1 (Fig. 4A), in which hardly any propulsion is produced (Fig. 4B,C,F), reducing the mean acceleration of the start. However, if the zebrafish detects the threat sufficiently early, it can initiate stage 1 of the fast start to begin stage 2 at the optimal moment. Hence, the relatively long duration of stage 1 without significant propulsion might not be a disadvantage for zebrafish larvae when escaping from predators.

Contributions of stage 1 and stage 2

Stage 1 is necessary to prepare the body for acceleration, but it takes up, on average, over half the time of a fast start without providing much propulsion (Fig. 4). The displacement is much larger in stage 2 (Fig. 4B), as is the peak speed, especially in the direction of the final heading (Fig. 4C). Stage 2 shows a larger linear momentum than stage 1 (Fig. 4D), as well as a larger peak force (Fig. 4F). In contrast, the angular momentum is often smaller in stage 2 than in stage 1 (Fig. 4E), despite the generally higher peak torques in stage 2 (Fig. 4G). The torques are more consistently in the direction of reorientation in stage 1, allowing the angular momentum to build to a higher value.

The role of stage 1 and stage 2 in the fast start has been the subject of on-going debate. The first stage has often been called purely preparatory (Domenici and Blake, 1997; Hertel, 1966; Weihs, 1973). Stage 1 prepares the body for stage 2: its preparatory role is clear (Fleuren et al., 2018). In addition to the preparatory function, it has also been argued that stage 1 may contribute significantly to propulsion (Fleuren et al., 2018; Tytell and Lauder, 2008; Wakeling, 2006). For bluegill sunfish, 37.2±0.6% of linear momentum is produced after stage 1 (Tytell and Lauder, 2008); for the larval zebrafish, this is somewhat lower at 27.8±8.2% (Fig. 5C). Based on the linear momentum, there is some propulsion component in stage 1, but the displacement, speed, peak linear momentum and peak forces are all considerably lower than in stage 2 (Fig. 4). Arguably, the preparatory role of the start, including reorientation, is more important for zebrafish larvae than the propulsive role.

Conclusions

In this article, we analysed the dynamics of the fast start of zebrafish larvae at 5 days post-fertilisation. We confirm that early-development larvae can produce effective escape responses in a wide range of directions (both azimuth and elevation) and speeds. The larvae seem to be able to adjust the direction and speed of their escape almost independently. They adjust the escape angle mostly with the extent of body curvature, while the escape speed is adjusted mostly with the duration of the start. Apart from its preparatory role, stage 1 is used to produce most of the reorientation, while stage 2 produces most of the acceleration of the centre of mass. This shows that despite their early stage of development, zebrafish larvae meet the functional demands for producing effective escape responses.

Acknowledgements

We thank the staff of the Carus fish facilities for providing the zebrafish larvae. We thank Kas Koenraads for his assistance during the experiments.

Competing interests

The authors declare no competing or financial interests.

Author contributions

Conceptualization: C.J.V., F.T.M., J.L.v.L.; Methodology: C.J.V., R.P.M.P., J.L.v.L.; Software: C.J.V., J.L.v.L.; Validation: C.J.V.; Formal analysis: C.J.V.; Investigation: C.J.V., R.P.M.P., J.L.v.L.; Resources: J.L.v.L.; Data curation: C.J.V.; Writing - original draft: C.J.V.; Writing - review & editing: C.J.V., F.T.M., J.L.v.L.; Visualization: C.J.V.; Supervision: F.T.M., J.L.v.L.; Project administration: C.J.V., R.P.M.P., F.T.M., J.L.v.L.; Funding acquisition: C.J.V., F.T.M., J.L.v.L.

Funding

This work was supported by grants from the Netherlands Organisation for Scientific Research (Nederlandse Organisatie voor Wetenschappelijk Onderzoek): NWO/ALW-824-15-001 to J.L.v.L. and NWO/VENI-863-14-007 to F.T.M.

Data availability

Data are available from the Dryad digital repository (Voesenek et al., 2019): dryad.gv43sm2

References

Ahlborn, B., Harper, D. G., Blake, R. W., Ahlborn, D. and Cam, M. (1991). Fish without footprints. *J. Theor. Biol.* **148**, 521-533. doi:10.1016/S0022-5193(05)80234-6

Borazjani, I., Sotiropoulos, F., Tytell, E. D. and Lauder, G. V. (2012). Hydrodynamics of the bluegill sunfish C-start escape response: three-dimensional simulations and comparison with experimental data. *J. Exp. Biol.* **215**, 671-684. doi:10.1242/jeb.063016

Butail, S. and Paley, D. A. (2012). Three-dimensional reconstruction of the fast-start swimming kinematics of densely schooling fish. *J. R. Soc. Interface* **9**, 77-88. doi:10.1098/rsif.2011.0113

Danos, N. and Lauder, G. V. (2007). The ontogeny of fin function during routine turns in zebrafish *Danio rerio*. *J. Exp. Biol.* **210**, 3374-3386. doi:10.1242/jeb.007484

Dobrovolskis, A. R. (1996). Inertia of any polyhedron. *Icarus* **124**, 698-704. doi:10.1006/icar.1996.0243

Domenici, P. and Blake, R. W. (1991). The kinematics and performance of the escape response in the angelfish (*Pterophyllum eimekei*). *J. Exp. Biol.* **205**, 187-205. doi:10.1139/z93-325

Domenici, P. and Blake, R. W. (1993). Escape trajectories in angelfish (*Pterophyllum eimekei*). *J. Exp. Biol.* **177**, 253-272.

Domenici, P. and Blake, R. W. (1997). The kinematics and performance of fish fast-start swimming. *J. Exp. Biol.* **200**, 1165-1178.

Domenici, P., Blagburn, J. M. and Bacon, J. P. (2011). Animal escapology I: theoretical issues and emerging trends in escape trajectories. *J. Exp. Biol.* **214**, 2463-2473. doi:10.1242/jeb.029652

Eaton, R. C. and Emberly, D. S. (1991). How stimulus direction determines the trajectory of the Mauthner-initiated escape response in a teleost fish. *J. Exp. Biol.* **161**, 469-487.

Eaton, R. C., DiDomenico, R. and Nissanov, J. (1988). Flexible body dynamics of the goldfish C-start: implications for reticulospinal command mechanisms. *J. Neurosci.* **8**, 2758-2768. doi:10.1523/JNEUROSCI.08-08-02758.1988

Ehrlich, D. E. and Schoppik, D. (2017). Control of movement initiation underlies the development of balance. *Curr. Biol.* **27**, 334-344. doi:10.1016/j.cub.2016.12.003

Eilers, P. H. C. (2003). A perfect smoother. *Anal. Chem.* **75**, 3631-3636. doi:10.1021/ac034173t

Fetcho, J. R. and McLean, D. L. (2010). Some principles of organization of spinal neurons underlying locomotion in zebrafish and their implications. *Ann. N. Y. Acad. Sci.* **1198**, 94-104. doi:10.1111/j.1749-6632.2010.05539.x

Fleuren, M., Van Leeuwen, J. L., Quicazan-Rubio, E. M., Pieters, R. P. M., Pollux, B. J. A. and Voesenek, C. J. (2018). Three-dimensional analysis of the fast-start escape response of the least killifish, *Heterandria formosa*. *J. Exp. Biol.* **221**, jeb168609. doi:10.1242/jeb.168609

Foreman, M. B. and Eaton, R. C. (1993). The direction change concept for reticulospinal control of goldfish escape. *J. Neurosci.* **13**, 4101-4113. doi:10.1523/JNEUROSCI.13-10-04101.1993

Gazzola, M., Van Rees, W. M. and Koumoutsakos, P. (2012). C-start: optimal start of larval fish. *J. Fluid Mech.* **698**, 5-18. doi:10.1017/jfm.2011.558

Hale, M. E., Long, , Jr, J. H., McHenry, M. J. and Westneat, M. W. (2002). Evolution of behavior and neural control of the fast-start escape response. *Evolution* **56**, 993-1007. doi:10.1111/j.0014-3820.2002.tb01411.x

Harper, D. G. and Blake, R. W. (1990). Fast-start performance of rainbow trout *Salmo gairdneri* and northern pike *Esox lucius*. *J. Exp. Biol.* **150**, 321-342.

Hertel, H. (1966). Fast start-trout. In *Structure, Form, Movement*, pp. 160-162. Reinhold Publishing Company.

James, R. S. and Johnston, I. A. (1998). Scaling of muscle performance during escape responses in the fish *Myoxocephalus scorpius* L. *J. Exp. Biol.* **201**, 913-923.

Kasapi, M. A., Domenici, P., Blake, R. W. and Harper, D. (1993). The kinematics and performance of escape responses of the knifefish *Xenomystus nigri*. *Can. J. Zool.* **71**, 189-195. doi:10.1139/z93-026

Li, G., Müller, U. K., Van Leeuwen, J. L. and Liu, H. (2012). Body dynamics and hydrodynamics of swimming fish larvae: a computational study. *J. Exp. Biol.* **215**, 4015-4033. doi:10.1242/jeb.071837

Li, G., Müller, U. K., Van Leeuwen, J. L. and Liu, H. (2014). Escape trajectories are deflected when fish larvae intercept their own C-start wake. *J. R. Soc. Interface* **11**, 20140848-20140848. doi:10.1098/rsif.2014.0848

Lucas, K. N., Dabiri, J. O. and Lauder, G. V. (2017). A pressure-based force and torque prediction technique for the study of fish-like swimming. *PLoS ONE* **12**, e0189225. doi:10.1371/journal.pone.0189225

Müller, U. K. and Van Leeuwen, J. L. (2004). Swimming of larval zebrafish: ontogeny of body waves and implications for locomotory development. *J. Exp. Biol.* **207**, 853-868. doi:10.1242/jeb.00821

Müller, U. K., Van den Boogaart, J. G. M. and Van Leeuwen, J. L. (2008). Flow patterns of larval fish: undulatory swimming in the intermediate flow regime. *J. Exp. Biol.* **211**, 196-205. doi:10.1242/jeb.005629

Nair, A., Azatian, G. and McHenry, M. J. (2015). The kinematics of directional control in the fast start of zebrafish larvae. *J. Exp. Biol.* **218**, 3996-4004. doi:10.1242/jeb.126292

Nair, A., Nguyen, C. and McHenry, M. J. (2017). A faster escape does not enhance survival in zebrafish larvae. *Proc. R. Soc. B Biol. Sci.* **284**, 20170359. doi:10.1098/rspb.2017.0359

Nelder, J. A. and Mead, R. (1965). A simplex method for function minimization. *Comp. J.* **7**, 308-313.

Schielzeth, H. (2010). Simple means to improve the interpretability of regression coefficients. *Methods Ecol. Evol.* **1**, 103-113. doi:10.1111/j.2041-210X.2010.00012.x

Simo, J. C. and Wong, K. K. (1991). Unconditionally stable algorithms for rigid body dynamics that exactly preserve energy and momentum. *Int. J. Numer. Methods Eng.* **31**, 19-52. doi:10.1002/nme.1620310103

Song, J., Zhong, Y., Luo, H., Ding, Y. and Du, R. (2018). Hydrodynamics of larval fish quick turning: a computational study. *Proc. Inst. Mech. Eng. Part C J. Mech. Eng. Sci.* **232**, 2515-2523. doi:10.1177/0954406217743271

Soto, A., Stewart, W. J. and McHenry, M. J. (2015). When optimal strategy matters to prey fish. *Integr. Comp. Biol.* **55**, 110-120. doi:10.1093/icb/icv027

Stewart, W. J., Cardenas, G. S. and McHenry, M. J. (2013). Zebrafish larvae evade predators by sensing water flow. *J. Exp. Biol.* **216**, 388-398. doi:10.1242/jeb.072751

Stewart, W. J., Nair, A., Jiang, H. and McHenry, M. J. (2014). Prey fish escape by sensing the bow wave of a predator. *J. Exp. Biol.* **217**, 4328-4336. doi:10.1242/jeb.111773

Stickel, J. J. (2010). Data smoothing and numerical differentiation by a regularization method. *Comput. Chem. Eng.* **34**, 467-475. doi:10.1016/j.compchemeng.2009.10.007

Tytell, E. D. and Lauder, G. V. (2008). Hydrodynamics of the escape response in bluegill sunfish, *Lepomis macrochirus*. *J. Exp. Biol.* **211**, 3359-3369. doi:10.1242/jeb.020917

Van Huffel, S. and Vandewalle, J. (2006). *The Total Least Squares Problem: Computational Aspects and Analysis*. Philadelphia, Pennsylvania, USA: Society for Industrial and Applied Mathematics.

Van Leeuwen, J. L., Voesenek, C. J. and Müller, U. K. (2015). How body torque and Strouhal number change with swimming speed and developmental stage in larval zebrafish. *J. R. Soc. Interface* **12**, 20150479. doi:10.1098/rsif.2015.0479

Van Raamsdonk, W., Pool, C. W. and Te Kronnie, G. (1978). Differentiation of muscle fiber types in the teleost *Brachydanio rerio*. *Anat. Embryol.* **153**, 137-155. doi:10.1007/BF00343370

Voesenek, C. J., Pieters, R. P. M. and Van Leeuwen, J. L. (2016). Automated reconstruction of three-dimensional fish motion, forces, and torques. *PLoS ONE* **11**, e0146682. doi:10.1371/journal.pone.0146682

Voesenek, C. J., Muijres, F. T. and Van Leeuwen, J. L. (2018). Biomechanics of swimming in developing larval fish. *J. Exp. Biol.* **221**, jeb149583. doi:10.1242/jeb.149583

Voesenek, C. J., Pieters, R. P. M., Muijres, F. T. and Van Leeuwen, J. L. (2019). Data from: Reorientation and propulsion in fast-starting zebrafish larvae: an inverse dynamics analysis. *Dryad Digital Repository.* https://doi.org/10.5061/dryad.gv43sm2

Wakeling, J. M. (2006). Fast-start mechanics. In *Fish Biomechanics* (ed. R. E. Shadwick and G. V. Lauder), pp. 333-368. Academic Press.

Walker, J. A., Ghalambor, C. K., Griset, O. L., McKenney, D. and Reznick, D. N. (2005). Do faster starts increase the probability of evading predators? *Funct. Ecol.* **19**, 808-815. doi:10.1111/j.1365-2435.2005.01033.x

Webb, P. W. (1975). Acceleration performance of rainbow trout *Salmo gairdneri* and green sunfish *Lepomis cyanellus*. *J. Exp. Biol.* **63**, 451-465.

Weihs, D. (1973). The mechanism of rapid starting of slender fish. *Biorheology* **10**, 343-350. doi:10.3233/BIR-1973-10308

Wöhl, S. and Schuster, S. (2007). The predictive start of hunting archer fish: a flexible and precise motor pattern performed with the kinematics of an escape C-start. *J. Exp. Biol.* **210**, 311-324. doi:10.1242/jeb.02646

Zupan, E. and Saje, M. (2011). Integrating rotation from angular velocity. *Adv. Eng. Softw.* **42**, 723-733. doi:10.1016/j.advengsoft.2011.05.010